

Dynamic Pressure Sensitive Adhesion in Nematic Phase of Liquid Crystal Elastomers

Hiro J. Farre-Kaga, Mohand O. Saed, and Eugene M. Terentjev*

The correlation between the anomalous mechanical dissipation and the pressure-sensitive adhesion in nematic liquid crystalline elastomers (LCEs) is explored, comparing hard glassy and soft materials (high and low crosslinking density, respectively) and nematic versus isotropic genesis. Two significant factors are identified contributing to strong adhesion: the intrinsic damping, which is high in the nematic phase, and the surface roughness, which is affected by the elastomer genesis. At the same time, it is found that surface energy plays only a minor role in pressure-sensitive adhesion. Theoretical calculations of dynamic adhesion are carried out by summing over the full range of frequencies in the dynamic-mechanical master curves data, and by averaging over surface roughness in soft and hard regimes, the results fitting the measured data with quantitative accuracy. Finally, the adhesion strength in LCEs altered by controlling the nematic phase temperature range is demonstrated.

The characteristics of a damping material are reflected in the linear complex modulus $E^*(\omega)$ at a given oscillation frequency ω , characterized by its real and imaginary parts: the storage and loss moduli E' and E'' , and their ratio E''/E' , usually referred to as the loss factor $\tan\delta$ with δ the phase angle of complex E^* . The loss factor $\tan\delta$ is directly related to the other parameters describing damping: $\tan\delta = 2\zeta = 1/Q$, where the “quality factor” Q and the “damping ratio” ζ are commonly used in the analysis of resonance circuits. The striking feature of liquid crystalline elastomers (LCEs), well studied in the equilibrium regime, is their “soft elasticity”, which manifests as a wide plateau of low nearly-constant stress upon increasing strain, and is caused by internal rotation of the local director axis,

1. Introduction

Pressure sensitive adhesives (PSA) are an important application of viscoelastic polymers,^[1,2] which generally provide quick adhesion after applying light pressure, without chemical reactions or solvent evaporation, and subsequent detachment in some situations. There is a strong relationship between the adhesion characteristics and the dissipative element of the mechanical response, which we will explore in detail here. In general, a polymer has fixed properties, its surface being either sticky or non-sticky, and this varies only slightly and monotonically with the environmental conditions such as humidity or temperature. Dynamically switchable adhesion is therefore an important target in materials design. Many systems have been proposed to have a (desirably) sharp transition of adhesive characteristics in response to various stimuli, including thermal, pH, electric, chemical, etc.^[3] with most of them relying on surface topography and chemical functionality. Recently, we have proposed a different method to impart dynamically switchable adhesion characteristics,^[4] exploring the anomalous mechanical damping of liquid crystalline elastomers.^[5]

absorbing applied strain without elastic energy cost.^[6,7,8] The related “dynamic soft elasticity” of nematic LCE^[9,10,11] is seen in the unusual aspects of dynamic-mechanical response, and in particular, the anomalous attenuation of acoustic waves propagating in LCE,^[12] caused by strong mechanical damping which increases with vibration frequency.^[5] On the other hand, as the LCE is heated into the isotropic phase, the anomalous damping ends and one finds the usual $\tan\delta = 0.1\text{--}0.2$ of ordinary rubbers. Here we study the PSA aspect of nematic LCE and correlate it with their anomalous dissipation via the link between $\tan\delta$ and the adhesion force.^[13,14,15]

From the materials point of view, we examine the effect of crosslinking density by comparing a soft 10% crosslinked LCE to a hard 80% crosslinked LCE. From the processing point of view, we examine the effect of network “genesis”: the LCE crosslinked in the isotropic phase and then cooled down into the nematic (isotropic genesis) and the LCE crosslinked directly in the nematic phase (nematic genesis).^[16] Accordingly, we have four materials to study, labelled as LCE10(i,n) and LCE80(i,n) reflecting their crosslinking and genesis.

Surface roughness is known to strongly affect adhesion strength as it increases the contact area.^[17,18,19] The polydomain LCE of isotropic genesis will have a smooth surface in the isotropic phase, but will develop a significant surface roughness in the nematic phase, as its misaligned domains each elongate in random directions. On the other hand, the nematic-genesis LCE will have the smooth surface in the nematic phase, but will develop roughness on heating into the isotropic phase, for the same reason of domains locally changing their shape with respect to their natural crosslinking configuration. This effect

H. J. Farre-Kaga, M. O. Saed, E. M. Terentjev
Cavendish Laboratory
University of Cambridge
JJ Thomson Avenue, Cambridge CB3 0HE, UK
E-mail: emt1000@cam.ac.uk

 The ORCID identification number(s) for the author(s) of this article can be found under <https://doi.org/10.1002/adfm.202110190>.

DOI: 10.1002/adfm.202110190

is an additional factor to the change in internal viscoelastic damping that will affect the adhesion strength.

In contrast to the two significant factors mentioned above, the surface energy is known to be largely unchanged across different LCE phases (which is confirmed through contact angle measurements reported in Figure S3, Supporting Information). So, since we see a large enhancement in adhesion in the nematic phase, the conclusion has to be that the equilibrium surface energy plays a minor role in the dynamic adhesive response.

Because of several logical threads followed here, this paper is organized as follows. We first discuss the effect of viscoelasticity and damping, presenting the results of adhesion force measurement depending on time of adhesion, the speed of probe pull-off, and the temperature. The details of the theory correlating adhesion and $\tan\delta$, and the fitting of

our data, are given in the Supporting Information. We then explore the role of surface roughness, and the change in surface roughness on transitions between nematic and isotropic phase in different-genesis systems. Again, the theory and the detailed fitting of our data, are relegated to the Supporting Information.

After testing several measuring methods, we have settled on the standard pull-test [probe-tack ASTM D4541 method] using a spherical steel probe, where we could more precisely control the deformation inflicted by the Hertzian indentation and avoided complications of non-parallel surfaces. **Figure 1** illustrates the test, and explains the definitions of adhesion force F_a , the vertical load applied and the adhesion time. The work done to detach the probe from the sample per unit area, referred to as adhesion energy, is calculated using $\gamma = Av/S$, where A and v

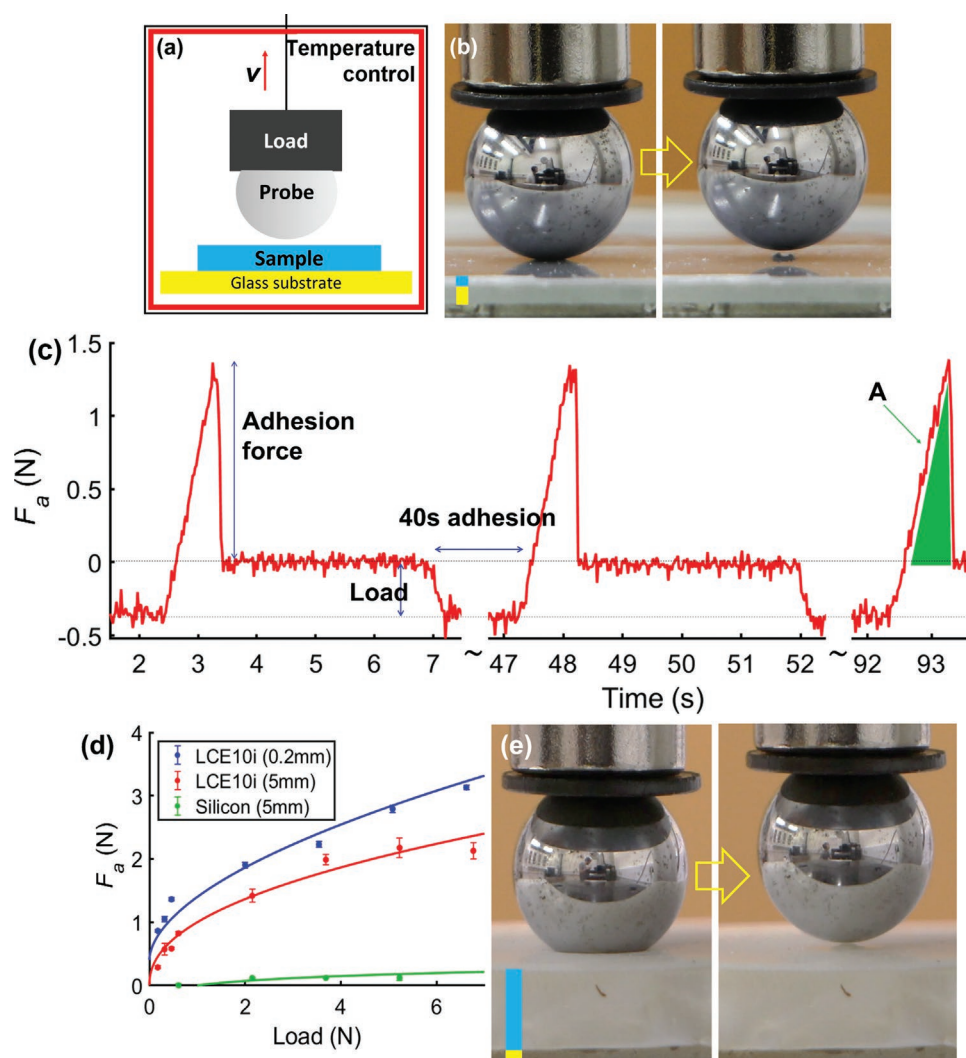


Figure 1. Experimental setup for dynamic adhesion. a) Scheme of apparatus with steel probe radius $r = 5$ mm and variable load. b) The thin LCE layer with the spherical probe pressing down, and then detaching. Note the shallow depression, and the neck of the adherent elastomer on detachment. The same material in a thick layer, in panel e), allows a much deeper indentation of the probe, and a wider-area deformation on detachment. c) Example of data collected from probe-tack tests. d) The plot illustrating adhesion force as function of load, for thick and thin LCE pads, also comparing with the silicone layer as reference. e) An illustration of probe-tack test on a thick layer of LCE, highlighting a much deeper indentation and a lack of necking on pull-off.

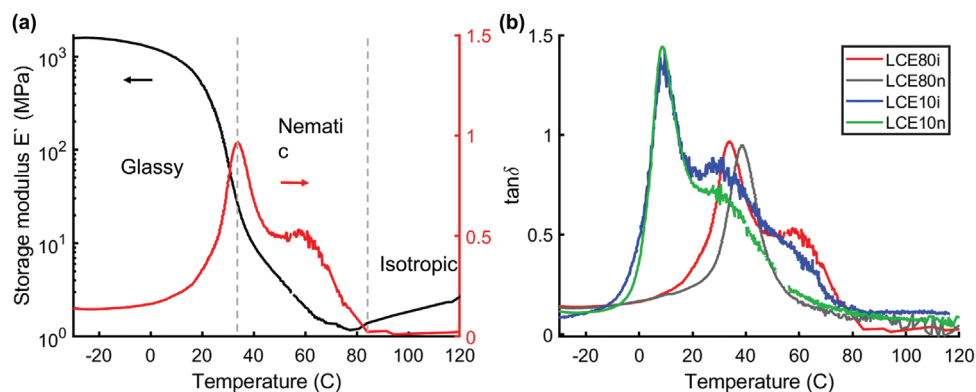


Figure 2. Dynamic mechanical analysis (DMA) results at 1 Hz. a) The example storage modulus E' and $\tan\delta$ traces of LCE80i, at 0.02% strain oscillation at 1 Hz. b) Comparing the $\tan\delta$ traces for all tested samples, supporting the data in Table 1.

are labelled in Figure 1, and S is the contact area between the probe and sample. After testing the effect of layer thickness, cf. Figure 1d, we did most of our experiments with the thin layer of LCE (0.2 mm), although this has prevented us from reaching very high loads (when the probe crushes through the thin layer). A constant load of 0.5 N was used for all other measurements. In Figure S3 (Supporting Information) we demonstrate the recovery of the LCE layer after the load-adhesion-pull-off sequence. These are thermoset elastomers, and although the layer does get a memory of the probe impact, a simple annealing has fully reset the LCE layers to their pristine pre-test condition.

2. Effect of Viscoelastic Relaxation

Viscoelastic materials show stronger adhesion because the total pull-off energy per unit area, γ , is composed from the equilibrium surface energy (γ_0), but also the energy dissipated by the material during the pull-off at a given speed.^[13] The combined expression can be written in the common form

$$\gamma(\nu, T) = \gamma_0 [1 + f(\nu, T)] \quad (1)$$

where we factorized the equilibrium surface energy. The second term is determined by viscoelastic damping and is strongly dependent on pull-off speed and temperature. Note that γ must not be confused with the frequently used concept of “surface tension” which is more relevant on liquids and has little effect on LCEs.

While measuring the full work of adhesion gives a more complete image of the adhesive, this study mainly evaluates the force of detachment F_a as it is a more relevant value when considering applications. Force is also the direct measurement in our setup. The relationship between force and adhesion energy $\gamma(\nu, T)$ depends on the debonding mechanism, which remained the same in our measurements. Using $\gamma = Av/S$ where $A \approx \frac{1}{2} F_a \Delta t$ as outlined in Figure 1c, we obtain $\gamma [J m^{-2}] \approx 25 F_a [N]$ as the stable conversion factor between the adhesion energy and adhesion force, its value being mainly unchanged for different materials and different pull-off speeds.

We could not detect a meaningful thermal signature of the nematic-isotropic transition in some of our materials using the traditional methods of differential calorimetry. This is a known feature^[21] and is due to high internal constraints in some of the main-chain nematic elastomers. We used the dynamic-mechanical (DMA) signature of this (T_{NI}), and the glass transition (T_g), because studies of many other LCE systems where both calorimetry and dynamic-mechanical measurements are valid have shown their good correlation. The glass transition has a very clear and well-understood signature in DMA. The nematic phase in LCE is characterized by its “dynamic soft elasticity”,^[9,10] showing a high $\tan\delta$ and low storage modulus E' compared to a regular elastomer. Accordingly, we identify the nematic-isotropic transition T_{NI} as a temperature where $\tan\delta$ falls below 0.2 and remains unchanged as temperatures rise further, and at the same time, the storage modulus E' starts growing linearly with temperature, as in classical rubber elasticity. The characteristic peak of $\tan\delta$ at the dynamic glass transition is a well-established feature of DMA response. **Figure 2** illustrates these features, and **Table 1** characterizes the four samples used in this investigation.

Adhesive response to pull-off speed ν clearly reveals the importance of viscoelastic relaxation (**Figure 3**) with F_a values increasing by over a factor of 3 in the speed range studied. Speed measurements of over 5 mm s⁻¹ could not be taken accurately due to the sampling rate limitations, and high-speed measurements on the tougher LCE80s could not be made at all. The theoretical model fitting the measurements in Figure 3c is discussed in detail in Supporting Information, where we show how to estimate the total adhesion strength by summing the oscillating ($\tan\delta$) response at all frequencies, caused by the probe stretching the material at a speed ν . To achieve

Table 1. The list of transition temperatures of the four materials we compare.

| Material | T_g [C] | T_{NI} [C] |
|----------|-----------|--------------|
| LCE10n | 10 | 80 |
| LCE10i | 10 | 80 |
| LCE80n | 39 | 91 |
| LCE80i | 34 | 85 |

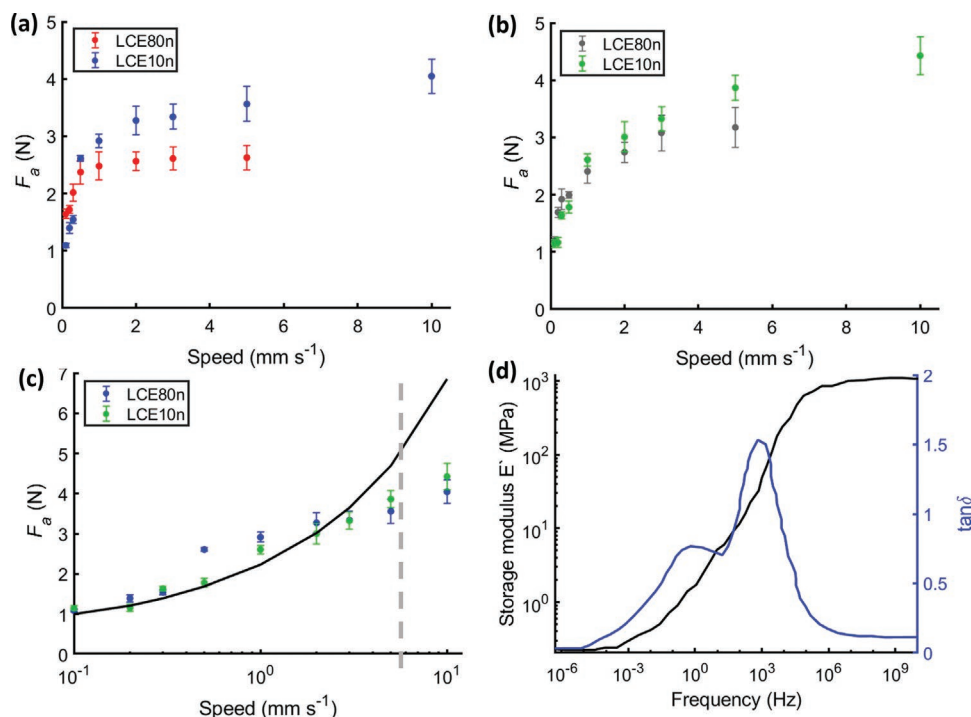


Figure 3. Adhesive response to pulling speed at room temperature showing the importance of viscoelasticity. a,b) Comparison of all samples, grouped in pairs by genesis. c) Linear-log plot of both LCE10(i,n) with the theoretical dynamic adhesive curve. The high-speed measurements beyond the dotted line were difficult to control and are considered unreliable. d) DMA Master Curves for LCE10i, at a reference temperature of 20°C, used in the calculation of the dynamic adhesive model. Notice the similarity with temperature ramp measurements in Figure 2 validating the time-temperature superposition.

such frequency integration, we have to use the Master Curves obtained by the time-temperature superposition, which allow projecting the response to super-high and super-low frequencies that can never be probed by experiment, Figure 3d. The reader unfamiliar with Master Curve characterization of viscoelastic materials should address the foundation texts [22,23] or look for details of how this method works in LCE.[9,24]

Fitting of the theoretical expression to the speed dependence given in Equation S2 in the Supporting Information requires the optimal parameters: the equilibrium crack tip radius $a_0 = 1$ mm, and the equilibrium modulus $E_0 = 0.15$ MPa, both imminently reasonable values. These results show that LCE10 has the equilibrium surface energy: $\gamma_0 = 25$ J m⁻².

An alternative, empirical relation between the dynamic part of adhesion energy and $\tan\delta$ is $f(v,T) \approx k \tan\delta(\omega,T)$, resulting in a version of the equation for adhesion energy of the form $\gamma(v,T) \approx \gamma_0 [1 + k \tan\delta(\omega,T)]$. Figure 4 illustrates this proportionality by examining the adhesion data obtained in our “standard” test with the vertical load of 0.5 N, and pull-off speed 0.3 mm s⁻¹, equilibrating at each temperature. Plotting the adhesion force and $\tan\delta$ on the same graphs shows that the high $\tan\delta$ of the nematic LCE phase has a direct and significant effect on the adhesion force. We found the proportionality constant k approximately the same in all materials, but different crosslink densities lead to different additive constants γ_0 , caused by additional factors including material hardness and surface roughness. This shows the significant drop in adhesion force between the nematic and isotropic phases for all materials other than LCE80n, which has almost no clear nematic

transition. The measured adhesion force plateaus at high temperature, when $\tan\delta \rightarrow 0$, is at 0.2 and 0.45 N for LCE80 and LCE10, respectively, implying the equilibrium surface energy γ_0 of 5 J m⁻² for LCE80 and 10 J m⁻² for LCE10. These values are much lower than the γ_0 obtained in the dynamical testing in Figure 3, which may highlight the limitations of this empirical proportionality, or merely reflect that the sum over frequency modes was done from the Master Curve at the reference 20°C, while the plateau is tested at high temperature in the isotropic phase. Nevertheless, the main message is clear: as soon as the elastomer enters the nematic phase, the PSA strength on it increases by a factor of at least 3 – with the exception of the LCE80n system, which is over-crosslinked in the low-temperature phase and is not able to experience the nematic-isotropic transition, nor show enhanced adhesion.

The last point requires a discussion. The consistently low values of the adhesion force on LCE80n, seen in Figure 4a, may appear in contradiction to the data in Figure 3b, where the same material showed F_a of up to 3 N. The difference is in the pull-off speed, and it highlights the dynamic aspect of PSA effect we are investigating. Even though the loss factor $\tan\delta(\omega,T)$ of LCE80n does not have the added nematic damping at the 1 Hz, Figure 2b, higher pull-off speed would activate higher frequency modes in the material response (see Equation S2, Supporting Information) and consistently show high adhesion force on pull-off. One may conclude that the soft LCE10 materials could see applications as re-useable “sticky” tapes, while the hard LCE80n system is much better optimized to be a “gripper”, with little residual “stickiness” in quasi-static conditions.

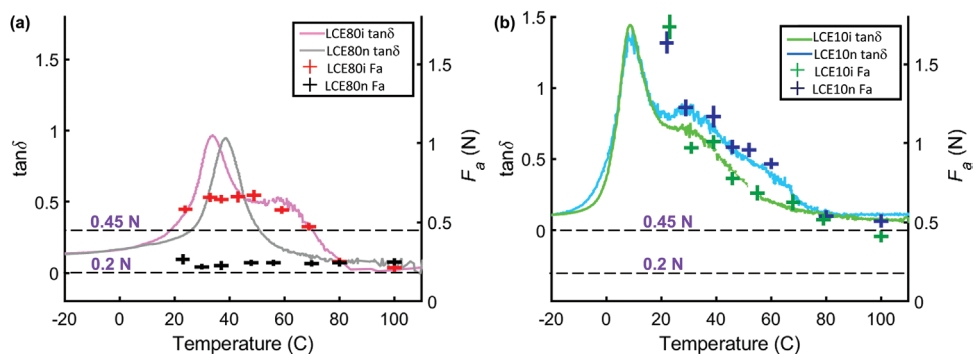


Figure 4. Adhesive dependence on temperature. There is a clear correlation between damping properties and adhesive energy for all samples, with both versions of LCE80 are plotted in a), and both versions of LCE10 in b). The crosses represent adhesion force measurements, and the continuous line in a lighter color shows the $\tan\delta$ measurements. The two high-temperature saturation levels of the adhesion force are reproduced in both plots for reference.

3. Effect of Surface Roughness

Two important physical factors are the real contact area between the probe and sample, and the energy cost of deforming the surface. Studies^[17] have modelled the effect of surface roughness on the adhesion energy by considering both the effect of contact area, contributing to $\chi(\nu, T)$ in the places where asperities touch the probe, and the elastic energy cost of deforming asperities, which does not depend on the speed of pull-off. Our experimental results show the overwhelming importance of viscoelastic effects, with force increasing to over 3 times from equilibrium, so the constant added value of deformation energy could be considered negligible.

However, the effect of surface roughness altering the effective contact area between the probe and sample makes an important contribution to adhesion strength. Nematic genesis materials have an increase in surface roughness when heated, as they change phase from smooth nematic to rough isotropic (and the isotropic genesis has the opposite effect). The

importance of this effect to provide a sharp transition in adhesion force is explored here. Experimental results in **Figure 5** show the dependence of the adhesion force on vertical load, giving rise to two important contact regimes which depend on the applied vertical load, roughness and the material hardness: the smooth regime where asperities are fully compressed, and the rough regime where only the tips of asperities contribute to contact area, as illustrated in sketches (c). The comparison of data with theoretical curves shows that both soft LCE10s have similar responses to load, with a crossover to the smooth regime at a vertical load of around 1 N regardless of their genesis. The harder LCE80s have a different response: the isotropic-genesis LCE80i (whose surface is naturally rough at room temperature) remains in the rough regime up to a limit of vertical load, that is, its asperities are never fully flattened. The nematic-genesis LCE80n remains in the smooth regime of adhesion, the brief appearance of lower adhesion force at very low vertical load is likely just a reflection of imperfect flatness (see Figure S5: Supporting Information).

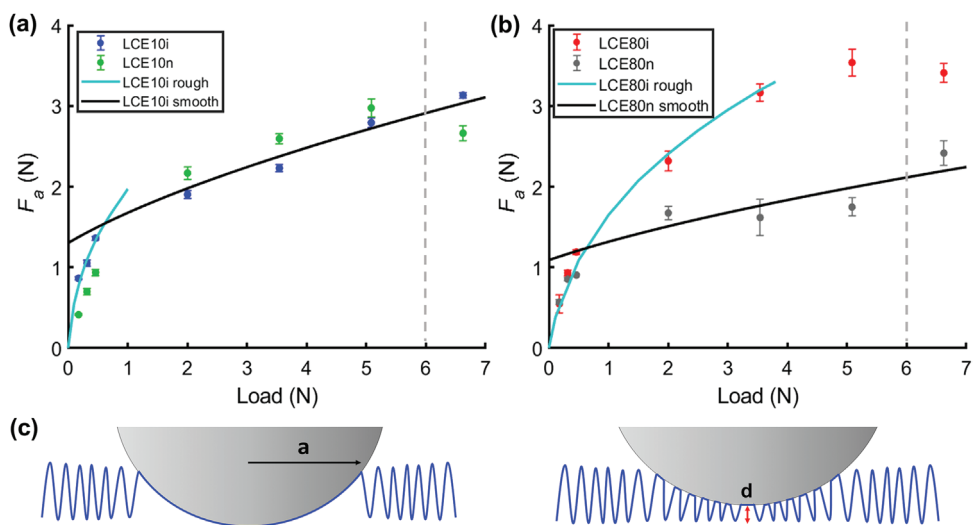


Figure 5. Adhesive response to increasing vertical load, and the effect of surface topography. a) LCE10 comparison. The two theoretical regimes accurately model the load response of both LCE10s, with the load crossover around 1 N. The LCE10n has a slightly lower F_a at low loads, caused by the smoother surface. The region to the right of the dotted line gave unexpected results, likely because the glass slide was bending at very high load. b) LCE80 comparison. The two have very different F_a at high load, due to their different topography combined with a higher rigidity. The nematic genesis quickly enters the smooth regime close to a plateau, due to its larger modulus compared to LCE10. The isotropic genesis remains well modelled by the rough regime even at high loads. c) Diagram illustrating the smooth regime (left), and the rough regime (right) of contact.

The best-fitted theoretical curves (using Equations S7 and S9; Supporting Information arising from the work in refs.[19,25,26]) used an equilibrium surface energy of 21 J m^{-2} for LCE10 and 30 J m^{-2} for LCE80, both of which are in the range of the separately measured energy γ_0 of 25 J m^{-2} , which was found by fitting the adhesion force to speed (Equations S1 and S2; Supporting Information). The difference between samples may be attributed to the larger real contact area of LCE80 in the nematic phase, as it was significantly smoother than LCE10.

These results show the important effect of surface roughness on adhesion strength, where an increased load (and therefore flattened surface asperities) significantly strengthens the adhesion. This suggests that a nematic genesis LCE will have an additional drop in adhesion strength when transitioning from the nematic phase (where their surface is naturally smooth) to the isotropic phase (where their surface becomes more rough).

4. Conclusion

This work confirms that soft nematic LCEs represent a novel and promising PSA system, with fine details of the adhesion process, and the choice of potential applications, depending on whether they are of nematic or isotropic genesis (i.e. having smooth or rough surface at room temperature). The comparison with isotropic PDMS in Figure 1d shows that adding the nematic order to a soft rubber imparts a significantly enhanced adhesion, and we found the direct correlation between the viscoelastic loss factor of the material and the PSA strength. All of the LCEs lose their added dynamic adhesion on heating above T_{NI} . A much better understanding is achieved for the mechanism of LCE adhesion, with a theoretical description accounting for the frequency spectrum of $\tan\delta$, and role of surface roughness flattening under vertical load, both of which accurately describe experimental data. Here we worked with thermoset networks, and confirmed that there was no permanent damage to the adhesive layer, which recovers its original characteristics after annealing, making the LCE a true multiple-use PSA system.

5. Experimental Section

Materials and Preparation of LCE: For preparation of LCEs, the methods reported previously were followed,^[21] with a single-step crosslinking reaction of thiol-acrylate Michael addition. The diacrylate monomer, 1,4-bis-[4-(3-acryloyloxypropyl)oxy] benzoyloxy]-2-methylbenzene (RM257) was purchased from Daken Chemical Co. The dithiol spacer, 2,2'-(ethylenedioxy) diethanethiol (EDDT), and tetrathiol crosslinker pentaerythritol tetrakis (3-mercaptopropionate) (PETMP), were purchased from Sigma Aldrich. Triethylamine (TEA, Sigma Aldrich) was used as the catalyst of the thiol-acrylate Michael-addition reaction. As the radical scavenger, butylated hydroxytoluene (BHT, from Sigma Aldrich) was used to suppress the unwanted radical polymerization reaction between acrylates, (see Figure S1; Supporting Information). All chemicals were used in their as-received condition with no purification. At the specific molar ratio of functional groups corresponding to the 10% or 80% crosslinking density, RM257, EDDT, PETMP, and BHT (0.5 wt%) were weighed. The Supporting Information gives a table with precise weight fractions. After each mixture was gently mixed at an elevated $T \approx 90^\circ\text{C}$ for ≈ 10 min, TEA was added at 0.8 wt% to start the Michael-addition reaction between thiol and acrylate groups.

The mixture was then transferred into a Teflon mold to complete the polymerization at 90°C (in isotropic phase) or at 20°C (in nematic phase) overnight. In this way the four materials were prepared: LCE10n and LCE10i for low crosslinking density, and LCE80n and LCE80i for high crosslinking density.

Adhesion Tests: The adhesion measurements used the home-made setup shown in Figure 1, which follows the probe-tack test standard ASTM D4541, programmed using a LabView software package. Peel tests were not used for the measurements as these are unsuitable for LCE materials: in a typical peel test (ASTM D3330) the strip of LCE is being pulled, which invokes a complicated mechanics of polydomain-monomodomain transition^[27] that would totally confuse the peel-force detection. A spherical probe was used to avoid misalignment between the sample and the probe. The load and probe were lowered to compress the sample for a constant adhesion time, and pulled off at a speed v . The effect of adhesion time on pull-off force plateaued after about 20 s, so the 40 s adhesion time was used in the investigation (Figure S2, Supporting Information). The load of 0.5 N was used in all constant-load tests. The pull-off force was measured with the home-made instrument using a stepper-motorized stage and an analogue load cell, reading the digitized data via the National Instruments data acquisition card. The sample was shifted after each detachment to avoid reattachment on a deformed surface (see Figure S4, Supporting Information). Such deformations disappear by heating the sample to an isotropic phase and re-cooling, showing the reversibility of the material's adhesion on annealing, which was also confirmed by over 10 heating-cooling cycles. Unusually low F_a measurements were discarded, as these were likely caused by dust accidentally covering the contact spot. The probe and sample were cleaned with ethanol after each set of measurements. As different samples had moduli ranging from 1 to 400 MPa, the amount of deformation would vary too widely with a thick sample, so all materials were prepared with a constant thickness of 0.2 mm. The speed of $v = 0.3 \text{ mm s}^{-1}$ was chosen for fixed- v tests as this activates enough frequency modes for viscoelastic energy loss to be significant, and is the interception point for all samples' speed response allowing closer comparisons to be made for other studied variables such as temperature.

Dynamic Mechanical Characterization: The small-amplitude oscillating measurements were carried out on TA DMA 850 instrument in tensile mode. The constant-frequency temperature scans were performed to identify the key phases of the materials (glass, nematic, isotropic rubber). For this the low frequency of 1 Hz was used to obtain the storage modulus closer to the expected equilibrium values of the Young modulus in different phases. The elevated values of the loss factor indicated enhanced mechanical dissipation across the nematic phase.

The time-temperature superposition was used to produce dynamic Master Curves of elastomers at a chosen reference temperature. As is standard in the WLF method,^[22,23] frequency scans were carried out in the available range of 0.01–200 Hz at different temperatures, and then scaled the frequency by a temperature dependent factor to achieve the overlapping of consecutive scans. This was successful across the glass transition (for which the WLF method is designed), however, crossing the nematic-isotropic transition makes it impossible to overlap the modulus curves since the overall modulus magnitude changes (downward) due to the nematic softness, and (upward) due to the entropic rubber-elastic effect on heating in the isotropic phase. The high-temperature data un-scaled across the nematic transition was left for the $E'(\omega)$ Master Curves. In contrast, the superposition of the loss factor worked perfectly across the nematic-isotropic transition.^[9,24]

Surface Topography Measurements

Surface scans were carried out on the Bruker Dektak XT using a $2 \mu\text{m}$ radius stylus, measuring at 0.1 mm s^{-1} , with the load of 0.1 N.

Supporting Information

Supporting Information is available from the Wiley Online Library or from the author.

Acknowledgements

This research was supported by European Research Council (H2020) AdG 786659. The authors are grateful for useful discussions with Takuya Ohzono.

Conflict of Interest

The authors declare no conflict of interest.

Data Availability Statement

The data that support the findings of this study are available from the corresponding author upon reasonable request.

Keywords

dynamic adhesion, liquid crystal elastomers, surface roughness, viscous dissipation

Received: October 8, 2021
Revised: November 15, 2021
Published online:

- [1] S. Moon, A. Chiche, A. M. Forster, W. Zhang, C. M. Stafford, *Rev. Sci. Instrum.* **2005**, *76*, 062210.
- [2] C. Creton, M. Ciccotti, *Rep. Prog. Phys.* **2016**, *79*, 046601
- [3] M. Kamperman, A. Synytska, *J. Mater. Chem.* **2012**, *22*, 19390.
- [4] T. Ohzono, M. O. Saed, E. M. Terentjev, *J. Adv. Mater.* **2019**, *31*, 1902642.
- [5] S. M. Clarke, A. R. Tajbakhsh, E. M. Terentjev, C. Remillat, G. R. Tomlinson, J. R. House, *J. Appl. Phys.* **2001**, *89*, 6530.
- [6] M. Warner, P. Bladon, E. M. Terentjev, *J. Phys. II* **1994**, *4*, 93.
- [7] S. M. Clarke, E. M. Terentjev, I. Kundler, H. Finkelmann, *Macromolecules* **1998**, *31*, 4862.
- [8] K. Urayama, R. Mashita, I. Kobayashi, T. Takigawa, *Macromolecules* **2007**, *40*, 7665.
- [9] A. Hotta, E. M. Terentjev, *Eur. Phys. J. E: Soft Matter Biol. Phys.* **2003**, *10*, 291.
- [10] E. M. Terentjev, A. Hotta, S. M. Clarke, M. Warner, *Philos. Trans. R. Soc. London, Ser. A* **2003**, *361*, 653.
- [11] D. R. Merkel, R. K. Shaha, C. M. Yakacki, C. P. Frick, *Polymer* **2019**, *166*, 148.
- [12] L. J. Fradkin, I. V. Kamotski, E. M. Terentjev, D. D. Zakharov, *Proc. R. Soc. London, Ser. A* **2003**, *459*, 2627.
- [13] B. N. J. Persson, O. Albohr, G. Heinrich, H. Ueba, *J. Phys.: Condens. Mater.* **2005**, *17*, R1071.
- [14] B. N. J. Persson, E. A. Brener, *Phys. Rev. E* **2005**, *71*, 036123.
- [15] F. Deplace, C. Carelli, S. Mariot, H. Retsos, A. Chateauminois, K. Ouzineb, C. Creton, *J. Adhesion* **2009**, *85*, 18.
- [16] J. S. Biggins, M. Warner, K. Bhattacharya, *J. Mech. Phys. Solids* **2012**, *60*, 573.
- [17] P. Lin, S. Vajpayee, A. Jagota, C. Hui, S. Yang, *Soft Matter* **2008**, *4*, 1830.
- [18] D. E. Packham, *Int. J. Adhes. Adhes.* **2003**, *23*, 437.
- [19] T. D. B. Jacobs, C. M. Mate, K. T. Turner, R. W. Carpick, *Understanding the Tip-Sample Contact*, Wiley, New York **2013**.
- [20] L. F. Kawashita, D. R. Moore, J. G. Williams, *J. Adhes.* **2006**, *82:10*, 973.
- [21] M. O. Saed, A. H. Torbati, C. A. Starr, R. Visvanathan, N. A. Clark, C. M. Yakacki, *J. Polym. Sci., Part B: Polym. Phys.* **2017**, *55*, 157.
- [22] J. D. Ferry, *Viscoelastic Properties of Polymers*, 3rd ed., Wiley, New York **1980**.
- [23] G. R. Tomlinson, in *3rd Int. Conf. on Intelligent Materials and 3rd European Conf. on Smart Structures and Materials*, Vol. 2779, International Society for Optics and Photonics **1996**.
- [24] M. O. Saed, W. Elmadih, A. Terentjev, D. Chronopoulos, D. Williamson, E. M. Terentjev, *Nat. Commun.* **2021**, *12*, 6676.
- [25] J. A. Greenwood, J. B. P. Williamson, *Proc. R. Soc. London, Ser. A* **1966**, *295*, 300.
- [26] B. Lorenz, B. A. Krick, N. Mulakaluri, M. Smolyakova, S. Dieluweit, W. G. Sawyer, B. N. J. Persson, *J. Phys.: Condens. Mater.* **2013**, *25*, 225004.
- [27] M. Warner, E. M. Terentjev, *Liquid Crystal Elastomers*, Oxford University Press, Oxford **2007**.